PVDF-Nanodiamonds Composite Membranes: Fabrication, Characterization and Water Treatment Applications

Asima Siddiqa[1*], Humaira Razzaq[1], Sara Qaisar[1], Sidra Liaqat[1,2], Arshad M[1], Rohama Gill[2]

[1]*NanoScience and Technology Department, National Centre for Physics, Islamabad, Pakistan*
[2]*Department of Environmental Sciences, Fatima Jinnah University, Islamabad, Pakistan*

ABSTRACT

Membrane forming ability of Polyvinyledenefluoride (PVDF) makes it of wider significance in membrane technology. However, hydrophobic nature of PVDF limits its application leading to the process of fouling. Different approaches are being employed to overcome this aforementioned issue. In the present study, novel PVDF/Nanodiamonds (NDs) nanocomposite membranes were formulated using solution casting technique using Dimethylformamide (DMF) as solvent. The morphology of the nanocomposite membranes were obtained by scanning electron microscope. The effects of addition of different weight percent of NDs (1-5 wt%) on shrinkage ratio, pure water flux, percentage of water content and porosity of the nanocomposite membranes were studied and results are discussed. It was established that with the increase in content into the nanocomposite membrane, the shrinkage ratio decreased while the pure water flux, water content and porosity of the membrane increased. Further, the applications of the PVDF/NDs nanocomposite membranes in separation of heavy metal ions from aqueous streams were also tested and the results are discussed.

Keywords: Poly(vinylidene fluoride), Nanodiamonds, Porosity, Shrinkage ratio, Water flux, Water content

INTRODUCTION

Water pollution has become a severe dilemma for all nations in the world, especially the underdeveloped and developing countries [1]. This then necessitates some process of water treatment which ensures the availability of clean water. Currently, membrane filtration technology has been acknowledged as a competitive candidate for separation, reclamation and reuse of water [2,3]. Membrane filtration processes are extensively employed in almost all industries, some of which are nuclear, food, chemical, and pharmaceutical production set-ups [4]. Membranes are an efficient alternate to the traditional processes of ultrapure water production, pathogen exclusion from water, desalination and solid-liquid separation in water treatment [5,6]. The performance of a membrane is directly related to its high penetrability and porosity, good stability and large hydrophilicity [7]. In this regard, the development of high-performance membranes based on Polypropylene (PP), Polytetrafluoroethylene (PTFE) and Poly(vinylidene fluoride) (PVDF) etc. to engineer the membrane properties has been extensively carried out [6-9]. Among these, PVDF is the most commonly employed polymer for applications in microfiltration, ultrafiltration and membrane distillation because of its inert behaviour towards chemicals, oxidants, UV and humidity. Also, PVDF is flexible and mechanically strong and can easily be cut and molded into shapes.

Nanocomposites based on PVDF exhibit a well-controlled porosity, exceptional chemical resistance, favourable thermal stability and excellent mechanical properties [10]. Furthermore, PVDF is polymorphic so that its properties can also be tuned by choosing the appropriate phase of the polymer. However, one of the major problems associated with the applications of PVDF membranes for waste water treatment is membrane fouling [11,12]. Fouling reduces the life of the membrane and also increases the cost of operation (efficiency) because of the blockage of pores by the deposit of salts or solution [11]. Due to its inherent hydrophobic nature, pristine PVDF membranes have the tendency to be contaminated by proteins, salts, oil, pathogens (virus, bacteria, etc.,) and some other impurities in the domain of waste water treatment [10-12] leading to a sharp decline of pure water flux and their permeability [13].

Currently, the main focus of research is to employ surface modification or blending modification methods to improve hydrophilic nature of the membrane. While surface modification methods are confined to the surface of the material, blending techniques modify the entire bulk. Blending techniques are based on chemical grafting, physical blending or addition of inorganic nanoparticles [14,15]. Literature reports on various bulk modification methods Mehwish et al. have reported membranes based on PVDF-SBS/MWCNT-Ag nanocomposite for water treatment [16]. Gopal et al. have reported better water flux and antifouling at a pressure of 0.5 bar for membranes based on PVDF and polysulfone [17].

V.R. Pereira used polyaniline nanofibers as hydrophilic additive to develop PVDF-PANI membrane which showed rejection for heavy metal ions i.e., Pb^{2+} and Cd^{2+} [18]. Jang et al. prepared porous PVDF/GO hybrid nanofiber membranes exhibiting pure water flux about 3 times higher and exceptional flux decline in comparison to neat PVDF nanofiber membrane [19]. Zhao et al. have studied the effect of GO on modified PVDF surface morphology, which is important for the separation process [20]. It has been reported that the addition of such fillers to the polymer matrix may lead to a better control of membrane surface properties, enhanced hydrophilicity and an increase in membrane permeability [15].

More recent trends are on the incorporation of carbon based materials such as graphene, graphite, fullerene, carbon fibers, carbon nanotubes, metal coated carbon fiber, carbon black and NDs into polymeric matrices [20,21]. NDs are spherical in shape, exhibit excellent electrical, thermal, mechanical and optical properties, have a rich surface chemistry, high surface to volume ratio, smaller size and are nontoxic in nature [21]. These unique properties of NDs make them superior in comparison to other carbon based nano fillers.

To the best of our knowledge, the role of NDs in rendering PVDF hydrophilic has not been reported so far. Herein, NDs were functionalized followed by incorporation into PVDF matrix as reinforcement material to fabricate nanocomposite microfiltration membrane by simple solution casting technique. Furthermore, various suitable techniques were employed to explore the physical features of the fabricated membranes. Also, changes in water flux upon stepwise addition of NDs into the nanocomposite membranes were investigated and correlated to the NDs content.

MATERIALS AND METHODS

Materials

PVDF powder ($M_r \sim 530000$) having density and average molecular weight of 1.74 g/cm^3 and molecular weight-534,000, respectively was obtained from Aldrich, USA. Commercial NDs with a purity of 95% and an average diameter of 50 nm were procured from Heyuan Zhong Lian Nanotechnology Co., Ltd, China. All other reagents including N,N-Dimethyl Formamide (DMF, ≥99%), Sulfuric Acid (H_2SO_4, ≥95.98%), Hydrochloric Acid (HCl, ≥37%) Nitric Acid (HNO_3, ≥70%), Sodium Hydroxide (NaOH, ≥99%) were purchased from Sigma Aldrich and were used in the as-received state.

Functionalization of NDs

A stepwise process was employed for the functionalization of the as-received NDs [22]. In the first step, NDs were oxidized with a 3:1 mixture of H_2SO_4 and HNO_3 at 90°C for 1 h, under constant stirring. The solution was filtered and washed repeatedly with deionized water. In the second step, the above treated NDs were poured into a mixture of H_2SO_4 and HNO_3 (9:1, respectively) and stirred for 3 days (at 90°C). The products were again filtered and washed with deionized water till a neutral pH was attained. The resultant mixture was then treated first with 0.1 M NaOH and then with 0.1 M HCl at 90°C for one hour. This was followed by washing with deionized water at ambient temperature till a neutral pH was attained. Finally, the mixture was dried in a vacuum oven for 24 h at 100°C.

Preparation of nanocomposite membranes

The development of pristine PVDF and the PVDF/NDs composite membranes was carried out by the solution casting technique. PVDF (1 g) was first dissolved in DMF by stirring at 60°C for 6 h. NDs in different weight ratios of (1-5 wt%) were then added into the homogenous and transparent PVDF solution. Each of the resultant mixtures was stirred at 60°C for 6 h to form a uniform dispersion which was then left to dry in an oven at 100°C for 24 h. Nomenclature used for the samples is 1 N-PVDF, 2 N-PVDF, 3 N-PVDF, 4 N-PVDF and 5 N-PVDF, respectively.

Characterization techniques

X-ray Powder Diffraction (XRD) analysis was carried out to evaluate the structural properties of the samples on a Panalytical 3040/60 X` pert PRO diffractometer using Cu (Kα) source in the range of 10° to 80° at scan rate and step time of 0.04 and 1 s/step, respectively. The surface morphology and porosity of the prepared samples was determined using FEGSEM (Quanta 600F). FTIR spectroscopic analysis was done for the surface functional group elucidation of nanocomposites in the range of 500-4000 cm^{-1} using 1000 Perkin Elmer. The % transmittance of the PVDF-ND composites was determined using double beam UV-Visible-NIR spectrometer (lambda 35) in the range of 200 to 1100 nm. Thermal Gravimetric Analysis (TGA) profiles were recorded to determine the thermal stability and phase transformation of the nanocomposites through TGA/DT Perkin–Elmer, USA. X-ray Photoelectron Spectroscopy (XPS) measurements were done using a Scienta-Omicron XPS instrument equipped with a micro-focused monochromatic Al K-Alpha X-ray source. The source was operated at 15 KeV, with a 400 µ spot size, Constant Analyzer Energy (CAE) 100 eV for survey scans and 20 eV for detailed scans. Charge neutralization was done by applying a combined low energy/ion flood source to dissipate the charging effects. Data acquisition for the XPS was performed with Matrix software and data analysis was performed with Igor Pro along with XPS fit procedures. The curve fitting of spectra was done using Gaussian-Lorentzia line shape after performing the Shirley background corrections.

RESULTS AND DISCUSSION

XRD analysis

XRD studies were conducted to assess the crystallinity in the synthesized nanocomposites because the crystalline structure of synthetic materials determines the final characteristics of the materials [23]. Figure 1 presents the XRD patterns of pristine PVDF, un-functionalized NDs, functionalized NDS and PVDF-NDs composites with varying amount of NDs from 1-5 wt% in the region 10-80°. On the profile of the ND particles, un-functionalized exhibit diffraction at 15.1°, 32.1°, 43.2° and 75.0° in 2, respectively [24]. The XRD pattern of un-functionalized exhibit the presence of both sp^3 and sp^2 carbon [21,22]. The peaks located at 43.2° and 75.4° correspond to sp^3 carbon while peak present at 15.1° is referred to sp^2 carbon [25].
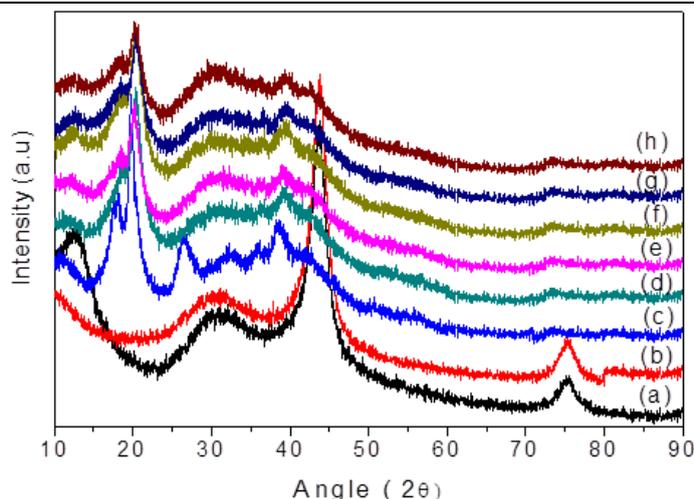
Figure 1: X-ray diffraction of (a) Un-functionalized nanodiamonds, (b) Functionalized nanodiamonds, (c) Pristine PVDF, (d) 1 N-PVDF, (e) 2 N-PVDF, (f) 3 N-PVDF (g) 4 N-PVDF and (h) 5 N-PVDF

However, the XRD pattern of functionalized NDs only exhibits the presence of sp^3 carbon which corroborates the removal of sp^2 carbon after functionalization [18,20]. Figure 2c and 2d-h are the diffraction patterns of pristine PVDF and PVDF-NDs composites with NDs contents from 1-5 wt%, respectively. The diffractograms of PVDF indicate diffraction peaks at values of 18.4°, 20.18° and 26.5°, 33.91°, 38.01° and 40.41° which can be assigned to (020), (110), (022), (131), (041) and (221) reflections of PVDF, respectively [23-25]. The XRD pattern of pristine PVDF identifies it as the β-phase of PVDF with monoclinic structure. However, with increase in the amount of NDs from 1-5 wt%, the increase in the area under the peaks and shifting of peaks towards higher angle is observed [26]. This indicates enhancement of crystalline phase of PVDF with the addition of NDs concentration [25,26]. The presence of a 2 peak around 75.0° in all nanocomposites implies that the NDs retain their crystalline structure even after being incorporated into the polymer matrix. This depicts the strong interaction between NDs and the polymer matrix [23].
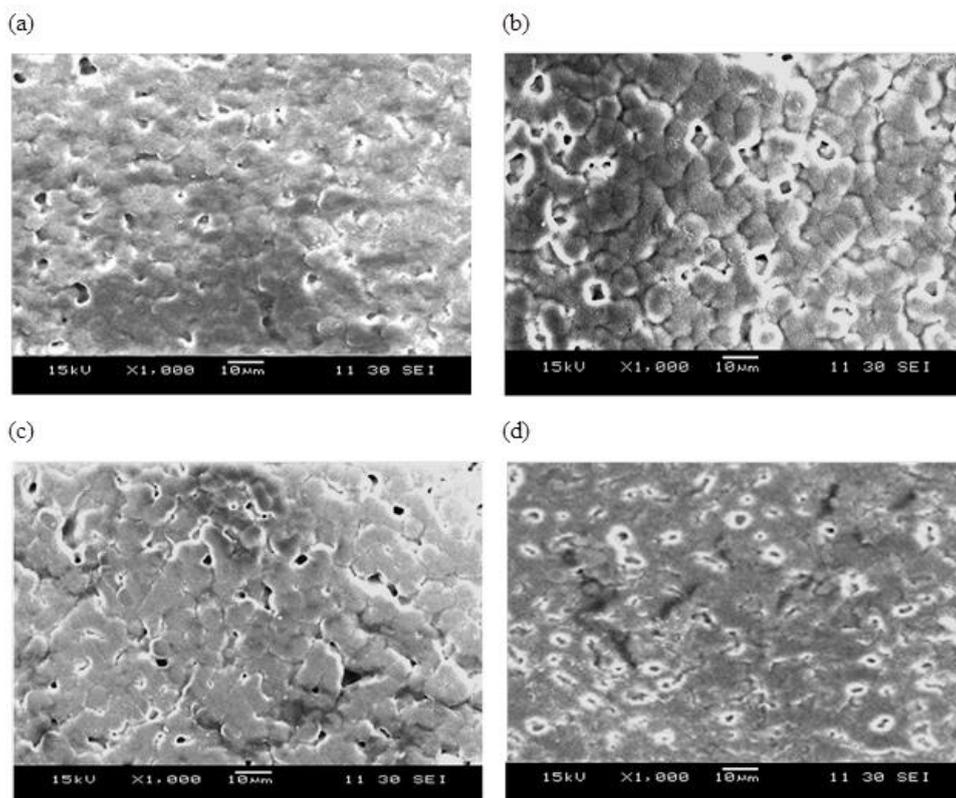

Figure 2: scanning electron microscope images of (a) Pristine PVDF, (b) 1 N-PVDF, (c) 3 N-PVDF and (d) 5 N-PVDF

SEM analysis

The morphological features of the membrane impart a vital role in the transportation of ions through the porous matrix and hence, in conductivity behavior. Figure 2 shows the SEM micrographs of the pristine PVDF and PVDF-NDs composite membranes i.e., 1 N-PVDF, 3 N-PVDF and 5 N-PVDF. It can be seen from Figure 2 that neat PVDF membrane (Figure 2a) exhibits visually the lower porosity while PVDF-NDs membrane with l wt.% NDs revealed slightly higher porous morphology than pristine. Also, a gradual increase in porosity with the addition of nano-filler content was observed and maximum porosity is obtained in membrane having 5wt% contents of NDs [11,12].

Moreover, these micrographs (Figure 2a-2d) also depicted a slight decrease in the average pore size from 6.1 to 1.7 μm with an increase in the filler loading which is attributed to an improved polymer/filler interaction [14]. In general, a high porosity and a small pore diameter are essential to boost the filtration effectiveness of the membranes [19].

FTIR studies

The FTIR spectra of the functionalized NDs and composite membranes (having 1 wt% NDs, 3 wt% NDs, 5 wt% NDs) were depicted in Figure 3a-3d, respectively. In the FTIR spectra of functionalized NDs, the band around 1630 cm^{-1} represents the characteristic feature of C=O group of COOH attributing to the bending vibration of physical absorbed water and hydrogen bonding, which arises from carboxylated group [13,14]. The broad absorption band between 3600 cm^{-1} and 3300 cm^{-1} is due to the OH functionality while the 1710 cm^{-1} band corresponds to C=O group [18,21]. This feature demonstrates the surface functionalization of the NDs by the acid treatment. However, the chemical structure of PVDF composite membranes (1 N-PVDF, 3 N-PVDF and 5 N-PVDF) is exhibited in Figure 3b-3d.
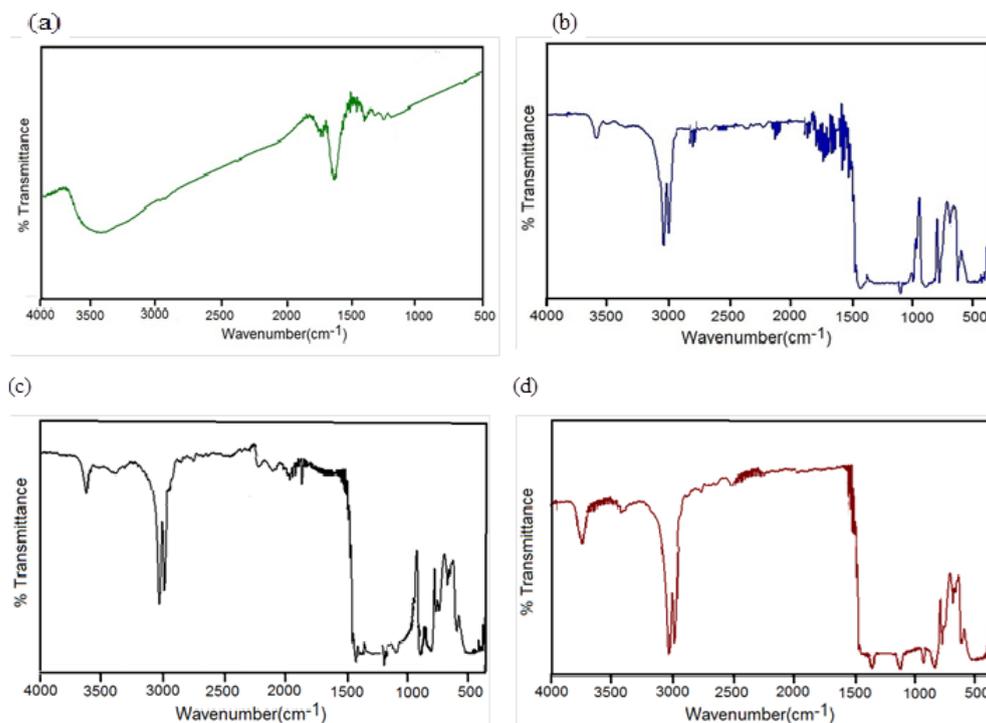

Figure 3: Fourier transforms infrared spectroscopy of (a) Functionalized nanodiamonds, (b) 1 N-PVDF, (c) 3 N-PVDF and (d) 5 N-PVDF

The bands located at 3080 cm^{-1} and 2985 cm^{-1} are assigned to the asymmetric and symmetric vibration CH$_2$ group of PVDF, respectively [16,19]. In all membranes, the small absorption peak present at 1403 cm^{-1} may be attributed to CH$_2$ wagging vibration. The band observed at 1185 cm^{-1} can be due to C–C band vibrations of PVDF [24,25]. The peaks positioned between 840-845 cm^{-1} and 870-880 cm^{-1} are related to C-F stretching vibration and C–C–C asymmetrical stretching vibration of PVDF [23]. The FTIR spectra of the composite membranes show that the incorporation of NDs does not affect the characteristic absorption peaks of the pristine PVDF membranes (Figure 3b-3d) [18,19]. Furthermore, composite membranes depict the presence of new bands between 3600 cm^{-1} and 3800 cm^{-1} and increased peak intensity for the functional groups [26]. The formation of these new absorption bands may be attributed to the O–H stretching vibration originating from the functional NDs [26,27]. These results indicate the successful embedment of the nanofillers in the composite membranes and it is in accordance with the XRD results (Figure 1). No other new peaks can be seen in the spectrum of composite membrane [25].

Transparency studies

Figure 4 shows the percent transmittance data of pristine PVDF and PVDF-NDs composites having NDs from 1-5 wt%. The % transmittance composites were determined using UV-Visible spectrophotometer in the wavelength range 200-1200 nm as shown in Figure 4. It can be observed from the data in Figure 4 that percent transmittance of all samples is increasing with the increase in wavelength of the radiation revealing the increase in the penetration power of electromagnetic radiation with increase in wavelength (nm) through the composites [25]. Furthermore, it can be seen from the figure that percent transmittance of the samples is gradually decreasing with the increase in NDs loadings from 1-5 wt%. These results depicts that the overall transparency of the composites vary with the incorporation of the filler, changing the system from translucent to opaque [26]. The membrane of pristine PVDF is translucent while the composites having NDs loadings 5 wt% is largely opaque. The % transmittances for pristine PVDF and composites having 1-5 wt% NDs exhibit a decreasing trend as the NDs are increased; ranging between 91% and 37%, respectively. This variation in the transmission reflects the effect of increasing concentrations of NDs on the opacity of the PVDF matrix [27,28].
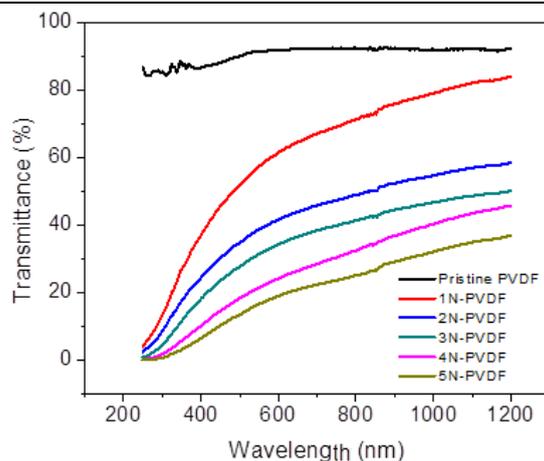
Figure 4: % Transmittance of pristine PVDF and PVDF-nanodiamonds composites with inclusion of 1-5% nanodiamonds

TGA analysis

TGA analysis of pristine PVDF, 1 N-PVDF, 3 N-PVDF and 5 N-PVDF was carried out to evaluate the effect of NDs on the thermal stability and mass loss behavior of PVDF as shown in Figure 5a-5d. Figure 5 shows that the thermal stability of polymer nanocomposites was enhanced with the addition of nanodiamonds from 1 wt% to 5 wt%. All nanocomposite membranes display similar degradation profile, representing one-step degradation pattern with smaller degradation pattern at higher temperature range. Pristine PVDF depicted thermo degradation around 490°C [23,24]. By increasing the NDs contents, the degradation temperature increased 490°C to 580°C with the incorporation of 5 wt% NDs. The first weight loss observed in all sample may be due to the oxidation of different organic groups in air relating to evolution of CO_2 and H_2O [29]. The smaller weight loss observed at higher temperature range may correspond to the decomposition of residual organic moieties and carbon contents in the membranes [30]. Consequently, the 5N-PVDF is found to be thermally more stable as compared to pristine PVDF. Increase in the filler concentration, the stability of the sample increased while the weight loss reduced which may be due to the increase in the interaction between the polymer matrix and the nanoparticles (nanodiamond) [28-30].
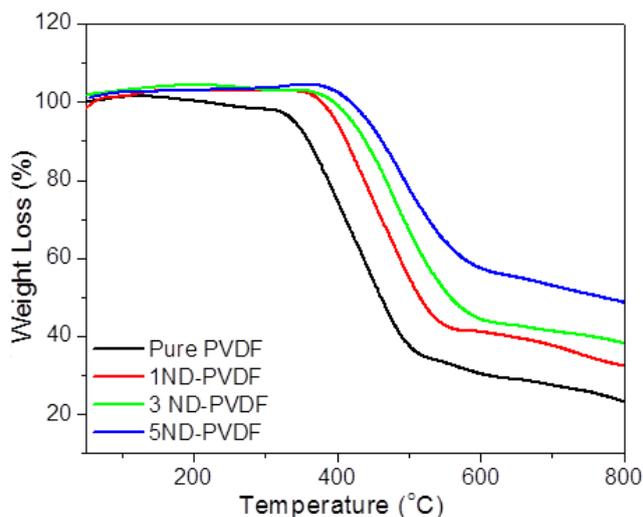

Figure 5: Thermo gravimetric analysis data of (a) Pristine PVDF, (b) 1 N-PVDF, (c) 3 N-PVDF and (d) 5 N-PVDF

XPS analysis

The XPS spectra collected for pristine PVDF and 5 N-PVDF is shown in Figure 6. The survey scan was obtained to identify the elements present on the surface of the sample. As expected this scan revealed the presence of carbon, oxygen and fluorine only. The detailed scans for Carbon (C1s), Oxygen (O1s) and Fluorine (F1s) core level spectra were collected for comprehensive analysis. The relative atomic percentages of carbon, oxygen and fluorine for pristine PVDF and 5 N-PVDF are shown in Table 1.

Table 1: Atomic percentage and fraction of peaks of pristine PVDF and 5 N-PVDF

Elements	Atomic percentage			Fraction of peaks
	C	O	F	CH_2/CF_2
Pristine PVDF	55.54	4.67	39.79	1
5 N-PVDF	63.15	9.55	27.3	1.9

Table 2: Percent solvent content of membranes in different solvents

Sample	Water	Methanol	Ethanol	Propanol
Pristine PVDF	2.01	1.01	0.4	0.32
1 N-PVDF	2.45	1.38	0.53	0.45
2 N-PVDF	2.73	1.5	0.79	0.58
3 N-PVDF	2.95	1.58	0.94	0.76
4 N-PVDF	3.1	1.67	1.2	0.95
5 N-PVDF	3.37	1.9	1.36	1.03

F1s spectra given in Figure 6b for pristine PVDF is resolved into two peaks at 688.13 eV and 689.2 Ev, which is attributed to the CH_2-CF_2 chemical structure [30]. The F1s peaks for 5 N-PVDF at 688.23 eV and 690 eV are assigned to CH_2-CF_2 and O-CFx, respectively. The C1s spectra for pristine PVDF membrane are deconvoluted into four sub peaks, which are leveled at 284.8 eV, 286.3 eV, 287.35 and 290.8 eV as represented in Figure 6c. The two main peaks; 286.3 eV and 290.8 eV are associated with CH_2 and CF_2 species, where 284.8 eV and 287.3 eV peaks are due to C-H/C-C and C-O, which shows the adsorption of oxygen or carbon from the environment [31]. The ratios of CH_2 and CF_2 components are 1, which is in agreement with chemical structure of PVDF. The C1s spectra for functionalized PVDF membrane are curve fitted with five peaks appearing at 285 eV, 286.45 eV, 288.3 eV, 291 eV and 292.35 eV [32]. The most prominent peaks at 285 eV, 286.45 and 291 eV are attributed to sp^3 carbon, CH_2 and CF_2, respectively [33]. The additional peak appearing at the higher binding energy edge at 292.35 eV characterize the CH_2-CF_2O bonding and a peak at 288.3 eV is observed due to the carbonyl groups [31,32].

Figure 6 shows the spectra of as received PVDF and 5 N-PVDF, the peaks are at 532.2 eV and 533.8 eV, which are assigned to C-O and O-F_x bondings [33]. The intensity of oxygen peaks is almost double for 5 N-PVDF in comparison to the intensity of as received PVDF. The increase in oxygen intensity is due to the hydroxy groups attached to NDs during functionalization [34].
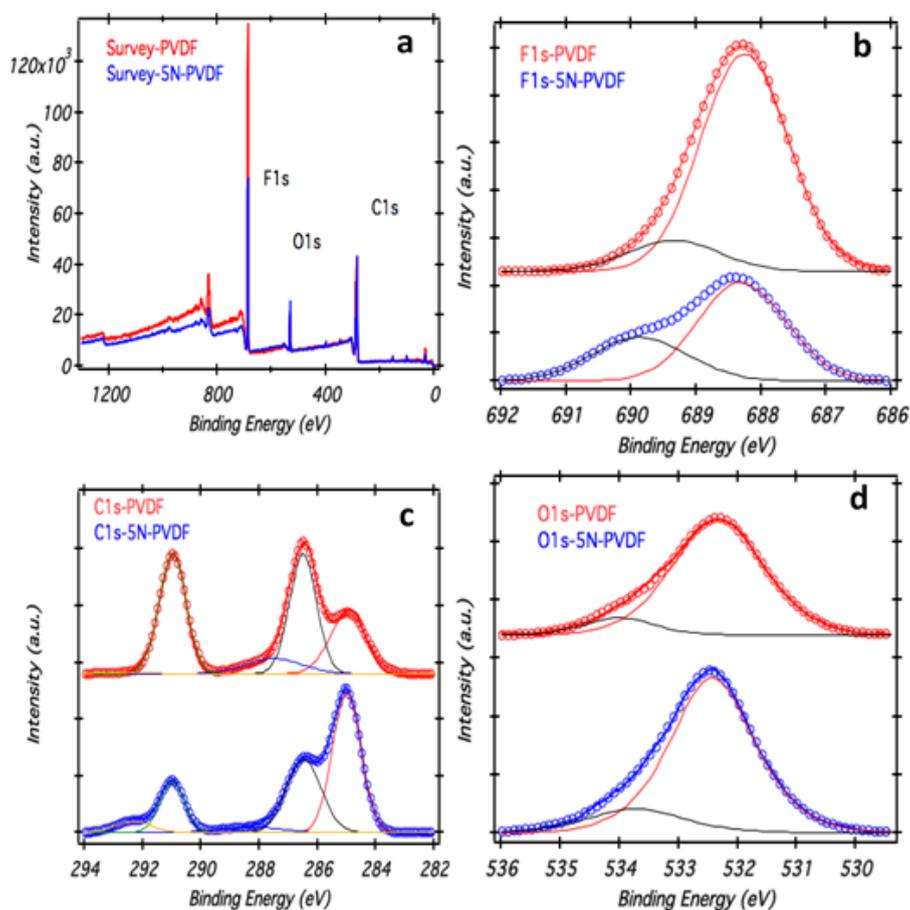

Figure 6: X-ray photoelectron spectra of pristine PVDF and 5 N-PVDF (a) Survey scan, (b, c and d) High resolution spectra of C1s, O1s and F1s core levels

Quantitative analysis of pristine PVDF shows that carbon and fluorine are the main components present on the surface along with a small amount of adventitious oxygen. In case of 5 N-PVDF the sp^3 carbon is present in abundant form, whereas the intensity of carbon peak associated to CH_2 and CF_2 has decreased tremendously [34]. The intensity of oxygen peak is almost twice in comparison to the pristine PVDF, the increase in the amount of the oxygen is due to the functionalized diamonds [32,33].

Analysis of porosity and pure water flux of membranes

For the determination of porosity and water contents of the PVDF-NDs membranes, the membranes samples were soaked in distilled water for 24 h which were later mopped with blotting paper and weighed. The wet membranes were dried at 100°C overnight and their weights were determined.

The apparent porosity of the membranes of the membranes (P) was determined as [35]:

$$Porosity\ (P) = (W_1 - W_2/A_h) \qquad (1)$$

Where, W_1 is the weight of wet membrane (g) and W_2 is dry membrane weight (g) and A_h is membrane area (cm^2).

For the determination of pure water flux of the membranes, the membrane was subjected to the pure water flux estimation at trans membrane pressure of 0.2 mbar. The permeability was determined under steady-state flow. Pure water flux was calculated by the following equation [36,37].

$$Pure\ water\ flux, J_w = \frac{Q}{A_t}, (ml.\,cm/min) \qquad (2)$$

The results of the porosity and pure water flux of the membranes are demonstrated in the Figures 7a and 7b, respectively. PVDF-NDs composite membranes illustrated steady increase in porosity with increase of NDs content from 1-5 wt%. These results are in accordance with the SEM images (Figure 2). It is known that PVDF is a polar polymer; that's why; the electrostatic repulsion between the chains may hinder the bundling of polymer chains thus leading to the formation of larger interconnected pores [35-37]. The inclusion of NDs may lead to the patterning of larger pores [36].
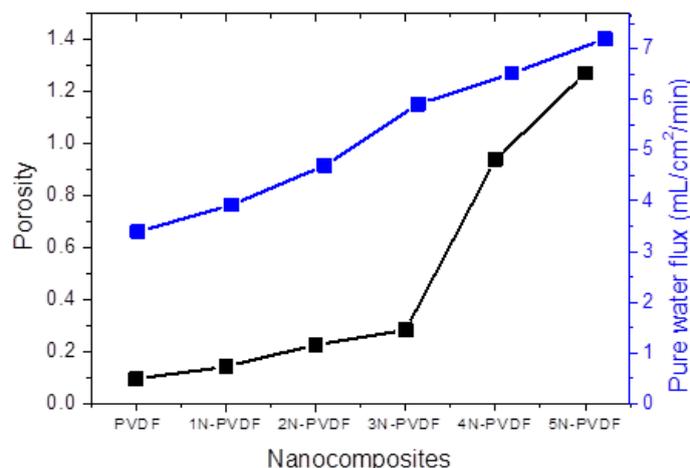

Figure 7a: Porosity and pure water flux of PVDF, 1 N-PVDF, 2 N-PVDF, 3 N-PVDF, 4 N-PVDF and 5 N-PVDF
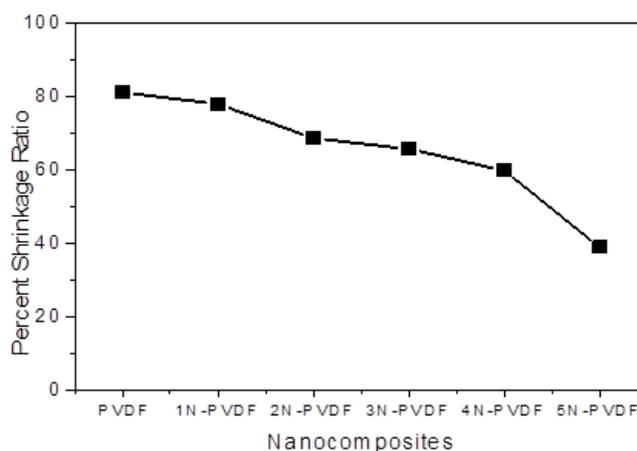

Figure 7b: Percent shrinkage ratio of PVDF, 1 N-PVDF, 2 N-PVDF, 3 N-PVDF, 4 N-PVDF and 5 N-PVDF

However, it was observed that pure water flux increased from 3.39-7.20 ml.cm/min from PVDF to 5 wt% NDs loaded PVDF composite membranes. These results are in accordance with the porosity and demonstrate linear relationship with the porosity [21,22]. Enhancement in the water flux plays a vital role in the nano-filtration properties of the membrane [28]. This increase in the water flux can be explained in terms of reduction in nucleation with the addition of the nanofiller which means that energy required to form critical size nucleus of PVDF reduces the crystalline nature of the polymer and thus resulting in the improvement of the water flux [36].

Analysis of shrinkage ratio and Percent solvent content of membranes

For the determination of shrinkage ratio, a piece of wet membrane was cut the length and width was measured. Then, the membrane was dried at 100°C and again its length and width were calculated. The shrinkage ratio was determined using following equation [36,37].

$$Shrinkage\ ratio\ (\%) = \left[1 - \left(\frac{a \times b}{ao \times bo}\right)\right] \times 100 \qquad (3)$$

Where, *a* and *b* are the length and width of the dry membrane (cm) and a_0 and b_0 are the length and width of the wet membrane (cm).

The increase in porosity with the addition of NDs has great impact on the shrinkage ratio of the membrane (Figure 7b), the higher the porosity, the lesser is the shrinkage ratio [28]. As can be seem from the Figure 7b, the increase in the nanofiller content from 1-5 wt%, the shrinkage ratio altered from 81%-38% in PVDF and PVDF-NDs with 5 wt% NDs. This emphasizes that PVDF-NDs composite membranes with 5 wt% filler content has minimum shrinkage ratio and maximum porosity and showed greater impact for use in water purification [30].

The percent water content of the membranes was determined for water, methanol, ethanol, propanol using following relationship [35] and results are demonstrated in Table 2.

$$Water\ content=(W_1-W_2/W_2) \qquad (4)$$

Where W_1 and W_2 are the weight of wet membrane (g) and dry membrane weight (g), respectively. It can also be observed from Table 3 that the increase in NDs concentration, the water content of the membrane increased which may be due to enhancement of hydrophilic nature and porosity of the membrane [25]. Whereas, the percent water content exhibited tremendous decrease when moving from water to propanol depending upon the hydrophilicity of the solvent. Therefore, the percent water content of all series increased with increasing the NDs concentration while decreased with the decrease in polarity of solvent [28,29].

Table 3: Percent solvent content of membranes in different solvents

Sample	Water	Methanol	Ethanol	Propanol
Pristine PVDF	2.01	1.01	0.4	0.32
1 N-PVDF	2.45	1.38	0.53	0.45
2 N-PVDF	2.73	1.5	0.79	0.58
3 N-PVDF	2.95	1.58	0.94	0.76
4 N-PVDF	3.1	1.67	1.2	0.95
5 N-PVDF	3.37	1.9	1.36	1.03

Salt rejection ratio and antifouling property

Salt rejection of the membranes was studied for zinc nitrate and copper acetate as per literature and shown in Table 2. The salt solution (0.1 M) was filtered through the membranes under pressure of 0.2 mbar. Filtrate was collected in order to study the rejection of the salt ions by membranes. Concentration of the salt in the feed and permeate was determined using conductivity meter. Percent salt rejection was calculated using the formula [30,31].

$$\%R=\left(1 - \frac{cp}{cf}\right) \times 100 \qquad (5)$$

Salt rejection of the membranes is depicted in Table 2. It can be seen that salt rejection increased with increase NDs level and is found to be higher for 5% N-PVDF nanocomposite membranes [25]. The percent salts rejection of the 5 N-PVDF membranes is in the range of 22.50-87.22% for copper acetate and 21.15-86.50% for zinc nitrate shown in Table 2.

The antifouling property of the nanocomposite membranes was studied as follows [3,25]. First of all, the pure water flux J_{w1} (ml/cm^2/min) of the membranes was measured at 0.2 mbar as described previously. For the evaluation of the antifouling property, zinc nitrate and copper acetate were taken as the model salts. An aqueous solution of each salt (0.1) was filtered through the membranes for 30 min under same pressure, separately. After the filtration, the membranes were flushed with pure water for 30 min and then the water flux J_{w2} (ml/cm^2/min) was measured again for each membrane. To determine the antifouling property of the membranes, the Fouling Recovery Ratio (FRR) was calculated by the equation, described below [36,37]:

$$FRR\ (\%)=\left(\frac{Jw1}{Jw2}\right) \times 100 \qquad (6)$$

The results of fouling recovery ratio of all membranes are demonstrated in Table 2. It can be noted that the FRR values of the membranes increased with NDs contents and FRR value of 5 N-PVDF membrane is higher than for both salts [38,39]. The high value of FRR value shows the better antifouling nature of the membranes. Membrane without any NDs, showed least FRR value due to the hydrophobic interaction between PVDF and aqueous solution of the salts [38]. Nevertheless better fouling resistance by membranes containing NDs indicated that the salts molecules adsorbed on the surface of membrane and deposited inside the pores during salts solution filtration were easily removed when the membranes were flushed with pure water. Therefore, from the FRR values and salt rejection ratio, it was evident that membranes with 5% NDs had better capacity for desalination and good antifouling nature than the pristine membranes [37-39].

CONCLUSION

This study has focused on the development of PVDF/NDs composite membranes for possible use in water filtration. Water filtration membranes based on pristine PVDF and its composites with NDs (1-5 wt%) have been prepared by the solution casting method. TGA results show that the enhanced interaction of the NDs with PVDF results in an increase in the stability of the nanocomposite membranes. Furthermore, as the NDs contents are increased, the degradation temperature shifts further to the higher side. Surface morphology and transmittance study of the synthesized membranes bear evidence to the homogenous dispersion of NDs into the blend, and to the complete embedment of the NDs into the PVDF matrix.

Study of membranes characteristics such as porosity, water content, pure water flux, shrinkage ratio, salt rejection and fouling recovery ratio reveal that PVDF membranes reinforced with NDs are better filters as compared to the pristine PVDF. The nanocomposite with 5 wt % NDs exhibits the best membrane properties. In summary, a facile approach to synthesize tunable hydrophilic porous membranes exhibiting good antifouling properties has been developed by the incorporation of NDs into the pristine PVDF matrix.

REFERENCES

[1] K. Yoon, B.S. Hsiao, B. Chu, *J. Mater. Chem.*, **2008**, 18, 5326-5329.
[2] M.A. Shannon, P.W. Bohn, M. Elimelech, *Nature*., **2008**, 54, 301-310.
[3] M.S. Diallo, J.C. Brinker, Science Policy Reports, *Springer*., **2011**.
[4] D.L. Arockiasamy, J. Alam, M. Alhoshan, *Appl. Water Sci*., **2013**, 3, 93-98.
[5] R. Kumar, K. Sharma, K.P. Tiwary, *Appl. Water Sci*., **2013**, 3, 285-290.
[6] N.S. Kotrappanavar, A.A. Hussain, M.E. Abashar, *Desalination*., **2011**, 280, 174-179.
[7] G.S. Ajmani, D. Goodwin, K. Marsh, *Water Res*., **2012**, 46, 564-570.
[8] Y. Yang, H.X. Zhang, P. Wang, *J. Membr. Sci*., **2007**, 288, 231-235.
[9] N. Shen, H.M. Ruan, L. Wu, *Chem. Eng. J*., **2011**, 168, 1272-1276.
[10] E. Fontananova, J.C. Jansen, A. Cristiano, *Desalination*., **2006**, 192, 190-195.
[11] J.R. Du, S. Peldszus, P.M. Huck, *Water Res*., **2009**, 43, 45594-5598.
[12] W. Zhou, A. Bahi, Y. Li, *RSC Adv*., **2013**, 3, 11614-11618.
[13] T. He, W. Zhou, A. Bahi, *Chem. Eng. J*., **2014**, 252, 327-330.
[14] H. Song, J. Shao, Y.B. He, *J. Membr. Sci*., **2012**, 405, 48-52.
[15] H. Wu, J. Mansouri, V. Chen, *J. Membr. Sci*., **2013**, 433, 135-140.
[16] M. Nabila, K. Ayesha, M. Siddiq, *Polym. Plast. Technol. Eng*., **2015**, 54, 474-483.
[17] R. Gopal, S. Kaur, Z.W. Ma, *J. Membr. Sci*., **2006**, 281, 581-590.
[18] R.P. Valeen, M. Arun, K.B. Udaya, *Desalination*., **2014**, 351, 220-225.
[19] J. Wongi, Y. Jaehan, J. Kyungsu, *RSC Adv*., **2015**, 46711-46715.
[20] C. Zhao, X. Xu, J. Chen, *Desalination*., **2014**, 340, 59-60.
[21] S. Mahdie, K. Alireza, V. Vahid, *Ind. Eng. Chem. Res*., **2014**, 53, 13370-13375.
[22] S.P. Bao, G.D. Liang, S.C. Tjong, *Carbon*., **2011**, 49, 1758-1762.
[23] N. Levi, R. Czrew, S.P. Xing, *Nano Lett*., **2004**, 4, 1267-1274.
[24] S. Manna, A.K. Nandi, *J. Phys. Chem. C*., **2007**, 111, 14670-11674.
[25] S. Devikala, P. Kamaraj, M. Arthanareeswari, *International Journal of Scientific and Research Publications.*, **2013**, 3, 1-5.
[26] S. Abbrent, J. Tegenfeldt, J. Plestil, *Polymer*., **2007**, 42, 1407-1410.
[27] M. Giovanni, V. Puergiorgio, P. Mariano, *Polym. Int*., **1996**, 41, 35-45.
[28] S. Osswald, G. Yushin, V. Mochalin, *J. Am. Chem. Soc.*, **2006**, 128, 11635-11639.
[29] S. Ansari, E.P. Giannelis, *J. Polym. Sci. Pol. Phys*., **2009**, 47, 888-892.
[30] S. Sotoma, K. Akagi, S. Hosokawa, *RSC Adv*., **2015**, 5, 13818-13823.
[31] L. Qian, L. Han-Han, W. Xiao-Lin, *Membranes*., **2014**, 4, 181-185.
[32] F.Y. Xie, W.G. Xie, L. Gong, *Surf. Interf. Anal*., **2010**, 42, 1514-1518.
[33] N. Akashil, S. Kuroda, *Polymer Letters*., **2015**, 9, 2-7.
[34] C. Jian-Hua, Z. Bao-Ku, J. Geng-Liang, *J. Membr. Sci*., **2005**, 266, 102-106.
[35] A. Kausar, A. Hussain, M.Y. Khan, *J. Plast. Film Sheet*., **2014**, 30, 314-318.
[36] E. Fontananova, J.C. Jansen, A. Cristiano, *Desalination*., **2006**, 192, 190-198.
[37] I. Mohmood, C.B. Lopes, I. Lopes, *Environ. Sci. Pollut. Res*., **2013**, 20, 1239-1243.
[38] K. Howe, M. Clark, *Environ. Sci. Technol*., **2002**, 36, 3571-3574.
[39] T. Carroll, S. King, S.R. Gray, *Water Res*., **2000**, 34, 2861-2865.